INSTITUTE OF PHYSICS PUBLISHING JOURNAL OF PHYSICS: CONDENSED MATTER

J. Phys.: Condens. Matter **17** (2005) 3537–3546 doi:10.1088/0953-8984/17/23/006

Lattice dynamics of high-pressure hydrogenated austenitic stainless steels

M Hoelzel[1], V Rajevac[1], S A Danilkin[2], T J Udovic[3], H Wipf[4] and H Fuess[1]

[1] Darmstadt University of Technology, Institute for Materials Science, Petersenstrasse 23, 64287 Darmstadt, Germany
[2] Bragg Institute, ANSTO, New Illawarra Road, Lucas Heights, NSW 2234PMB 1, Menai, Australia
[3] National Institute of Standards and Technology, NIST Center for Neutron Research, 100 Bureau Drive, MS 8562, Gaithersburg, MD 20899-8562, USA
[4] Darmstadt University of Technology, Institute for Solid State Physics, Hochschulstrasse 6, 64289 Darmstadt, Germany

Received 8 January 2005, in final form 16 March 2005
Published 27 May 2005
Online at stacks.iop.org/JPhysCM/17/3537

Abstract

The vibrational spectra of hydrogenated austenitic stainless steels AISI 304 (Fe/Cr18/Ni10) and AISI 310 (Fe/Cr25/Ni20) were investigated by inelastic neutron scattering. Based on the results of previous neutron diffraction studies, the data have been analysed by model calculations. The peaks corresponding to the optical modes show a significant broadening because of the variation of vibrational energies from one hydrogen site to another in the alloys. At high hydrogen contents (hydrogen-to-metal atomic ratios H/Me $\approx$ 1) the peak profile is dominated by hydrogen–hydrogen interactions. Correspondingly, the optical peaks show a splitting into longitudinal and transverse modes for H/Me $\approx$ 1. A continuous lowering of the vibrational energies with increasing hydrogen content was observed for both steels, reflecting a weakening of the hydrogen–metal interactions with increasing hydrogen–metal atomic distance.

1. Introduction

The effects of hydrogen on the structure and lattice dynamics of austenitic stainless steels are of particular interest because of hydrogen embrittlement. Addressing the various effects under consideration in the frame of hydrogen embrittlement in steels, particular attention has been paid to investigate hydrogen-induced phase transformations, hydrogen-induced weakening of atomic bonds and hydrogen-enhanced localized plasticity.

Previously, we reported on neutron diffraction studies to reveal the effects of hydrogen on the structure of 310 and 304 stainless steels (Hoelzel *et al* 2004). Hydrogenations have been carried out in a high-pressure cell at 623 K to achieve quite homogeneous hydrogen distributions at various hydrogen contents between H/Me = 0.3 and H/Me = 1. Rietveld

0953-8984/05/233537+10$30.00

Table 1. Results by neutron diffraction analysis on 310 steel (Fe/Cr25/Ni20).

Hydrogenation pressure (GPa)	Weight fraction of phases	Lattice constant at 80 K (Å)	Me–H interatomic distance (Å)	H-occupancy in octahedral sites (%)
2.3	100% $Fm\bar{3}m$	3.6586(1)	1.8293(1)	35 ± 2
3.0	100% $Fm\bar{3}m$	3.7261(2)	1.8631(1)	66 ± 3
7.0	100% $Fm\bar{3}m$	3.7798(2)	1.8899(1)	94 ± 5

refinement demonstrated that hydrogen occupies exclusively the octahedral interstitial sites in both steels. No phase transformations have been observed in 310 stainless steel for all investigated hydrogen contents up to H/Me ≈ 1, corresponding to a hydrogenation pressure of 7 GPa. In 304 stainless steel, the formation of ε-martensite has been detected after hydrogenation at 3.0 GPa, corresponding to H/Me $= 0.56$. The formation of ε-martensite was also found in 304 stainless steel subjected to a pressure of 4.0 GPa without hydrogen. Increasing hydrogen contents resulted in continuous lattice expansions of the austenite matrices in both steels. No reflections of possible hydride phases have been observed within detection limit in both steels. The phase transformation behaviour has been compared with electrolytically hydrogenated steels to consider the roles of hydrogen content and stresses due to different hydrogen-charging techniques.

Because of the large incoherent scattering cross-section of hydrogen, incoherent inelastic neutron scattering is very effective for the investigation of hydrogen vibrations in metals, offering information on metal–hydrogen interactions. Furthermore, inelastic neutron scattering can provide complementary information to neutron diffraction studies on hydride phases, in particular for low hydrogen contents or low volume fractions of hydride phases. In a previous inelastic neutron scattering study, the hydrogen vibrations in 310 stainless steel as well as in Fe/Cr18/Ni16/Mn10 stainless steel doped with H/Me $= 0.0033$–0.0037 have been investigated (Danilkin *et al* 2003). The energies of the fundamental mode and the second harmonics were found to be 130 and 260 meV, respectively, in both steels. Significant broadenings of the vibrational peaks have been attributed to the fact that the metal neighbours of hydrogen atoms vary from one hydrogen atom to another. The vibrational energies indicated an occupation of the octahedral interstitial sites.

In this work, we report on inelastic neutron scattering studies to analyse the vibrational spectra of the hydrogen-charged 310 and 304 stainless steels with high hydrogen contents from H/Me $= 0.3$ to 1. The studies have been carried out on exactly the same samples which had been investigated by neutron diffraction. Tables 1 and 2 present the results of neutron diffraction (Hoelzel *et al* 2004), which are important for the analysis of the inelastic neutron scattering studies.

2. Experimental details

Commercial AISI type 310 and AISI type 304 austenitic stainless steels were hydrogenated in a high-pressure cell at 623 K for 24 h. In general, hydrogenations at elevated temperatures for long charging times result in quite homogeneous hydrogen distributions since concentration gradients are removed by diffusion. The hydrogenations were performed in the Institute of Solid State Physics of the Russian Academy of Sciences in Chernogolovka (Moscow district). Each sample consisted of 3–6 discs of 8 mm diameter and 0.25 mm thickness. Pressures between 2.3 and 7.0 GPa were applied to obtain different hydrogen concentrations from H/Me $= 0.3$ to 1. In order to prevent the outgassing of hydrogen, the samples were stored at liquid nitrogen temperature.

Table 2. Results by neutron diffraction analysis on 304 steel (Fe/Cr18/Ni10).

Hydrogenation pressure (GPa)	Weight fraction of phases	Lattice constant at 80 K (Å)	Me–H interatomic distance (Å)	H-occupancy in octahedral sites (%)
2.3	100% $Fm\bar{3}m$	3.6537(1)	1.8269(1)	30 ± 2
3.0	84% $Fm\bar{3}m$	fcc:		fcc:
	16% $P6_3/mmc$	3.6988(2)	1.8494(1)	56 ± 2
		hcp:		hcp:
		$a = 2.617(2)$	1.848(2)	71 ± 9
		$c = 4.254(3)$		
7.0	Not analysed	fcc:		fcc
		3.7757(3)	1.8879(2)	103 ± 9
		hcp:		hcp:
		$a = 2.6676(8)$	1.883(1)	Not analysed
		$c = 4.335(2)$		

The inelastic neutron scattering studies were carried out at the filter-analyser neutron spectrometer (FANS) at the NIST Center for Neutron Research in Gaithersburg, MD. A Cu(220) monochromator was used to tune the energy of the incident neutrons. Collimators were set to 40′ divergence in front of the monochromator and 40′ divergence in front of the sample. The mean energy of neutrons passing the filter (Udovic *et al* 2004) was 1.2 meV. All measurements were carried out using a cryostat at 80 K. The samples were placed in a flat aluminium container. For each sample, the background due to fast neutrons was measured for various incident energies after placing cadmium in front of the analyser. The background scans resulting from interpolation of the various data points were subtracted from the corresponding measurements. Additional measurements of the empty sample container and of hydrogen-free steel samples demonstrated that the background predominantly resulted from fast neutrons.

3. Results and discussion

3.1. Fundamental optical vibrations

The vibrational densities-of-states have been calculated from the measured spectra. The multiphonon contribution to the spectra referring to simultaneous creations of optic and acoustic modes have been subtracted by applying the method of Dawidowski *et al* (1998). Figures 1 and 2 show the vibrational densities-of-states of hydrogen in 310 and 304 stainless steels, respectively, for various hydrogen concentrations. The peaks correspond to the fundamental optical modes. In figures 1 and 2, the data have been normalized so that the relative peak intensities match the hydrogen contents obtained in the previous diffraction studies (Hoelzel *et al* 2004). Obviously, samples of both steels with comparable hydrogen contents and, correspondingly, comparable metal–hydrogen atomic distances (tables 1 and 2), show very similar vibrational energies. An increasing hydrogen content is accompanied by a decrease in the vibrational energy, reflecting a softening of the metal–hydrogen interaction with increasing metal–hydrogen distance. Such a tendency has also been found in the fcc palladium–hydrogen system (Ross 1997). The vibrational energies of the fundamental modes indicate an occupancy of the octahedral interstitial sites (figure 3), in agreement with the diffraction studies (Hoelzel *et al* 2004). The sharp edges at about 75 meV could result from scattering from ice-Ih (Li and Kolesnikov 2002), since no correlation between these features and the hydrogen content of the samples has been found. As the samples weigh only 300–600 mg, even very small amounts of ice that can form during sample handling can give visible signals. Figure 3 illustrates the

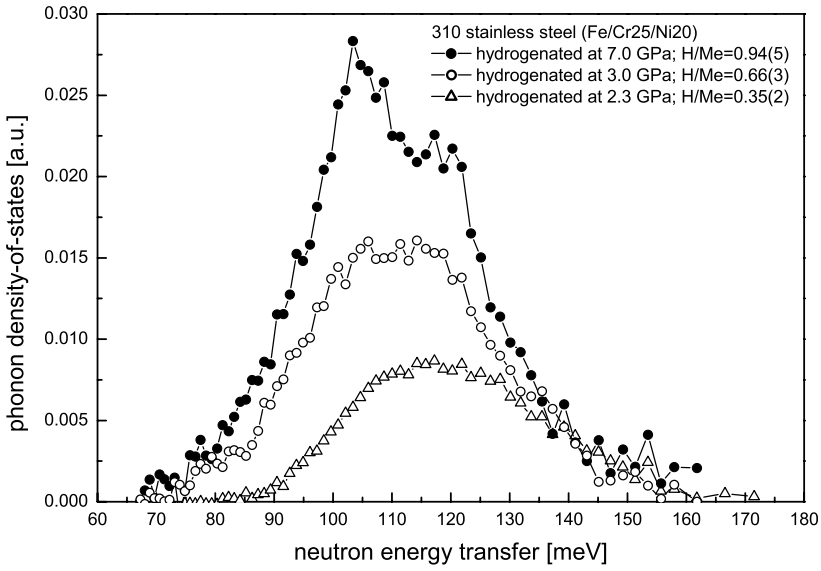

Figure 1. Phonon densities-of-states of hydrogenated 310 stainless steel at 80 K. The data have been corrected for background and multiphonon scattering. A normalization according to hydrogen content and sample mass has been performed.

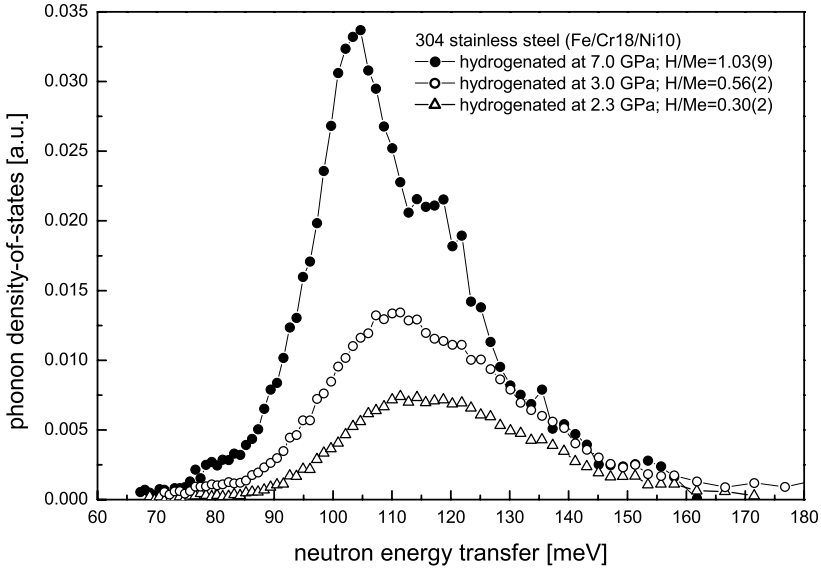

Figure 2. Phonon densities-of-states of hydrogenated 304 stainless steel at 80 K. The data have been corrected for background and multiphonon scattering. A normalization according to hydrogen content and sample mass has been performed.

vibrational energies of the fundamental modes as a function of metal–hydrogen atomic distance for 304 stainless steel ($Fm\bar{3}m$, this study), 310 stainless steel ($Fm\bar{3}m$, this study, Danilkin *et al* 2003), Fe/Cr18/Ni16/Mn10 stainless steel ($Fm\bar{3}m$, Danilkin *et al* 2003), ε-$FeH_{1.0}$ ($P6_3/mmc$, dhcp lattice, Cornell *et al* 1997), γ-$NiH_{1.05}$ ($Fm\bar{3}m$, Dorner *et al* 1989, Kolesnikov *et al*

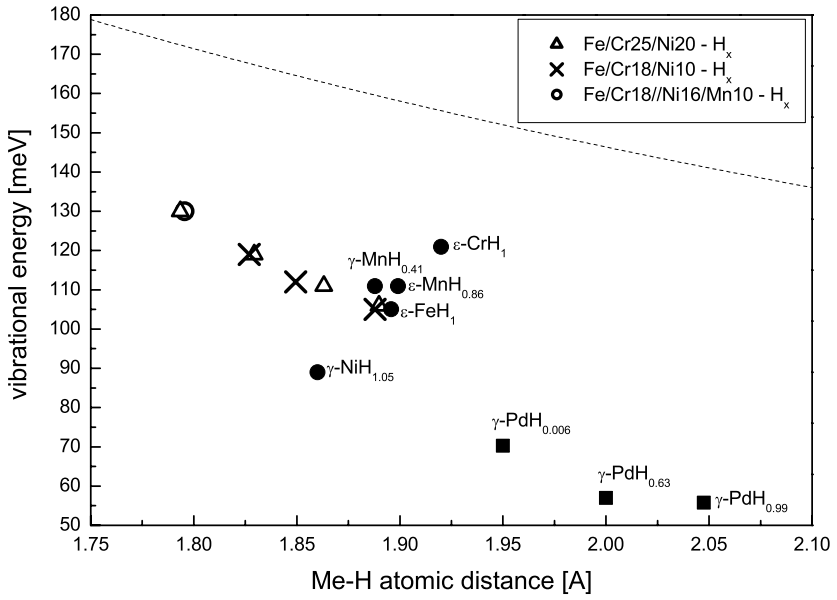

Figure 3. Vibrational energy of the fundamental optical mode versus metal–hydrogen distance for various hydrides of 3d-metals and palladium. The dashed curve presents a least-squares fit to data of fluorite-type dihydrides, given by Antonov *et al* (2000), for comparison.

1991), ε-CrH_1 ($P6_3/mmc$, Dorner *et al* 1989), ε-$MnH_{0.86}$ ($P6_3/mmc$, Kolesnikov *et al* 1991), γ-$MnH_{0.41}$ ($Fm\bar{3}m$, Antonov *et al* 2000), γ-$PdH_{0.006}$, γ-$PdH_{0.63}$ and γ-$PdH_{0.99}$ (palladium hydrides: $Fm\bar{3}m$, Ross 1997). For comparison with literature data, including the cited studies, the vibrational energies given in figure 3 have been derived from the maxima of the hydrogen vibrational modes. (The mean energies are generally slightly higher because of the asymmetric peak profiles.) The metal–hydrogen atomic distances have been derived directly from the lattice parameters. In dilute systems (H/Me $\ll$ 1) local metal–hydrogen distances are slightly higher than the values given by the lattice constants. In all systems, illustrated in figure 3, hydrogen atoms are supposedly located in the octahedral interstitial sites. In the case of the hexagonal hydrides (ε-$FeH_{1.0}$, ε-CrH_1, ε-$MnH_{0.86}$) the c/a ratios are close to the ideal ratio of $\sqrt{8/3}$, thus the hydrogen sites have cubic symmetry to a very good approximation. Therefore, the dynamical properties of d-metal hydrides with hcp structure and fcc structure could be considered jointly, as pointed out by Antonov *et al* (2000). The remarkable increase in the vibrational energies with increasing metal–hydrogen distance in the monohydrides of the 3d-metal series Ni $\rightarrow$ Fe $\rightarrow$ Mn $\rightarrow$ Cr has already been discussed by Antonov *et al* (2000). It indicates a strong increase in the metal–hydrogen–interactions because of the reduction of the number of valence electrons in this series, as predicted by Elsässer *et al* (1998). From figure 3 it can be seen that the vibrational spectra of 310 and 304 stainless steels with H/Me $\approx$ 1 follow this relationship.

In the case of hydrogen atoms occupying the tetrahedral interstitial sites in fcc metals, generally higher vibrational energies are observed for comparable metal–hydrogen atomic distances. For dihydrides with fluorite structure a monotonic decrease of the hydrogen vibrational energies with increasing metal–hydrogen atomic distance has been found (Ross *et al* 1979, Antonov *et al* 2000). In figure 3, a least-squares fit to data of fluorite-type dihydrides by Antonov *et al* (2000) is shown for comparison with the other data.

The spectra (figures 1 and 2) show a significant broadening of the optical modes in 310 and 304 stainless steels compared to the instrumental resolution (about 3 meV for 100 meV), quite similar to the spectra of 310 stainless steel and Fe/Cr18/Ni16/Mn10 stainless steel with very low hydrogen contents (H/Me = 0.0033 to 0.0037) (Danilkin *et al* 2003). The peak broadening in steels is much more pronounced than in the case of the pure metal hydrides ε-$FeH_{1.0}$, γ-$NiH_{1.05}$, ε-CrH_1, ε-$MnH_{0.86}$ and γ-$MnH_{0.41}$. In solid solutions of Fe, Cr and Ni the neighbourhood of metal atoms surrounding hydrogen varies from one hydrogen atom to another, resulting in a broad distribution of vibrational energies. Furthermore, the approximately random distribution of different metal atoms leads to a distortion of the octahedra around hydrogen atoms, resulting in a break of isotropy of interatomic potential as well as anharmonicity.

A splitting of the peaks corresponding to fundamental optical vibrations occurs at hydrogen contents close to H/Me = 1 in both steels (figures 1 and 2). As no phase transformations have been detected by neutron diffraction in 310 stainless steel even for Me/H = 0.94 (Hoelzel *et al* 2004), the splitting is supposedly related with strong hydrogen–hydrogen–interactions, resulting in transverse and longitudinal modes. In 304 stainless steel, the situation is more complicated, as the formation of ε-martensite with hcp structure has been detected for hydrogen contents H/Me > 0.56 in the diffraction studies. Nevertheless, the difference in the vibrational energies between the hcp and fcc phase might be very small, taking into account ε-$MnH_{0.86}$ and γ-$MnH_{0.41}$ (Antonov *et al* 2000). Thus, in 304 stainless steel with H/Me = 1.03, the splitting of the vibrational peaks supposedly results from dispersion, while the profile results from an overlapping of hydrogen modes in fcc and hcp lattices.

The formation of a fcc γ^* hydride phase as precipitates in the austenite lattice has been proposed based on x-ray diffraction studies on electrolytically hydrogenated 310 and 304 stainless steels (Narita *et al* 1982, Ulmer and Altstetter 1993). In the diffraction studies of the high-pressure hydrogenated 310 and 304 stainless steels, no reflections of a γ^* hydride phase have been observed (Hoelzel *et al* 2004). Also, the inelastic neutron scattering spectra (figures 1 and 2) do not give evidence for the coexistence of a γ^* hydride phase with the austenite matrix. In case of a miscibility gap, a splitting of vibrational peaks into two parts would be expected for corresponding H/Me ratios, while the relative peak intensities should vary with the hydrogen content. According to the continuous shift of vibrational energies with hydrogen contents, no evidence exists for a hydride formation in the high-pressure hydrogenated steels. High-pressure hydrogenations result in more uniform hydrogen distributions and lower internal stresses compared to electrolytical chargings (Hoelzel *et al* 2004). These effects could explain the discrepancy illustrated by the formation of γ^* hydride in high-pressure or electrolytically hydrogenated samples.

3.2. Modelling of vibrational modes

The spectra of steels with maximum hydrogen contents (H/Me $\approx$ 1) have been analysed based on Born–von Karman interactions to describe the peak profiles. The parameters corresponding to the metal–metal force constants have been derived from previous analysis of phonon dispersion measurements on austenitic stainless steels (Rajevac *et al* 2004). The expected softening of metal–metal interactions because of hydrogen-induced lattice dilatation has been estimated by the Grüneisen parameter. In these calculations, the steels have been treated as pure metal hydride with rock salt structure. Only nearest neighbour interactions, referring to metal–hydrogen, metal–metal and hydrogen–hydrogen interactions, have been taken into account. The vibrational densities-of-states, derived from the calculated phonon dispersion branches, have been convoluted with the instrumental broadening for a comparison with the experimental data. The calculated densities-of-states have been fitted to the experimental

Table 3. Parameters for the modelling of the hydrogen vibrational peaks for 304 (Fe/Cr18/Ni10) and 310 (Fe/Cr25/Ni20) stainless steels with H/Me ≈ 1. Averaged atomic masses have been used for the metal atoms: $m = 55.437$ for 304 stainless steel and $m = 55.452$ for 310 stainless steel. A resolution function with FWHM = 3 meV has been used for convolution.

Table 3.1. Force constants (in N m^{-1}) describing metal–metal interactions in both steels. The data have been taken from the analysis of phonon dispersion measurements (Rajevac *et al* 2004). For this purpose only nearest neighbour interactions were considered and the hydrogen-induced lattice expansion was taken into account using a Grüneisen parameter of $\gamma = 2.0$.

Notation	Interaction	Value (N m^{-1})	Parameter status
α_1	ϕ_{xx} (1/2, 1/2, 0) Me–Me	37.5	Fixed
β_1	ϕ_{zz} (1/2, 1/2, 0) Me–Me	7.0	Fixed
γ_1	ϕ_{xz} (1/2, 1/2, 0) Me–Me	42.3	Fixed

Table 3.2. Force constants (in N m^{-1}) describing metal–hydrogen and hydrogen–hydrogen interactions for 304 stainless steel (Fe/Cr18/Ni10), regarding the steel as pure monohydride MeH.

Notation	Interaction	Value (N m^{-1})	Parameter status
α_2	ϕ_{xx} (1/2, 0, 0) Me–H	51.6	Refined
α_3	ϕ_{xx} (1/2, 1/2, 0) H–H	6.4	Refined
β_3	ϕ_{zz} (1/2, 1/2, 0) H–H	−0.3	Refined
γ_3	ϕ_{xz} (1/2, 1/2, 0) H–H	5.4	Refined

Table 3.3. Force constants (in N m^{-1}) describing metal–hydrogen and hydrogen–hydrogen interactions for 310 stainless steel (Fe/Cr25/Ni20), regarding the steel as pure monohydride MeH.

Notation	Interaction	Value (N m^{-1})	Parameter status
α_2	ϕ_{xx} (1/2, 0, 0) Me–H	48.4	Refined
α_3	ϕ_{xx} (1/2, 1/2, 0) H–H	6.4	Refined
β_3	ϕ_{zz} (1/2, 1/2, 0) H–H	1.6	Refined
γ_3	ϕ_{xz} (1/2, 1/2, 0) H–H	6.7	Refined

Table 3.4. Hydrogen vibrational energies (in meV) used for the calculation of metal–hydrogen force constants. The second column gives values obtained from pure metal hydrides. The third and fourth columns present the corresponding vibrational energies after interpolation to actual metal–hydrogen atomic distances in 304 and 310 stainless steels with H/Me ≈ 1.

		Fe/Cr18/Ni10	Fe/Cr25/Ni20
Fe–H	From ε'-FeH_1 (Cornell *et al* 1997): 105	105	105
Ni–H	From γ-$NiH_{1.05}$ (Kolesnikov *et al* 1991): 89	87	87
Cr–H	From ε-CrH_1 (Dorner *et al* 1989): 121	124	124

Table 3.5. Force constants (in N m^{-1}) describing metal–hydrogen and hydrogen–hydrogen interactions for 304 stainless steel (Fe/Cr18/Ni10), considering the variation of vibrational energies because of the different metal atoms surrounding hydrogen atoms.

Notation	Interaction	Value (N m^{-1})	Parameter status
α_2	ϕ_{xx} (1/2, 0, 0) Me–H	43.3–64.4[a]	Fixed
α_3	ϕ_{xx} (1/2, 1/2, 0) H–H	6.4	Refined
β_3	ϕ_{zz} (1/2, 1/2, 0) H–H	0	Refined
γ_3	ϕ_{xz} (1/2, 1/2, 0) H–H	6.4	Refined

values by iterative modification of metal–hydrogen and hydrogen–hydrogen force constants. Table 3 gives an overview of the fixed and refined parameters used for the modelling.

In further model calculations, the variation of vibrational energies because of the different metal atoms has been considered. For this purpose, the configuration probabilities of six atoms from Fe, Cr and Ni surrounding one hydrogen atom have been calculated for both

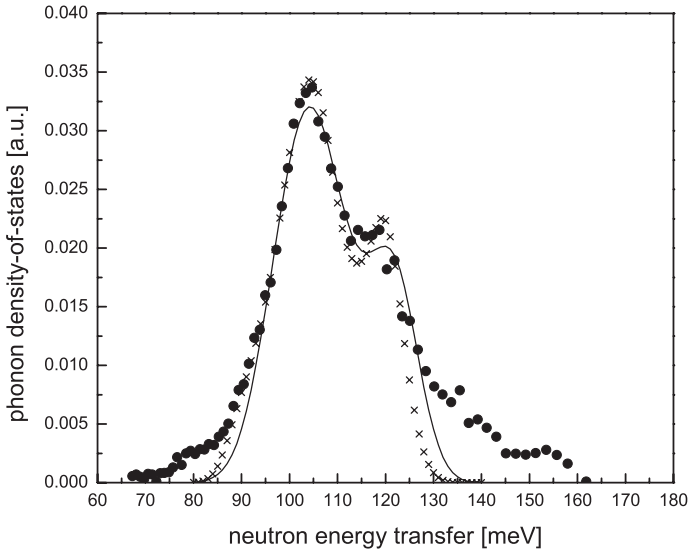

Figure 4. Phonon density-of-states of 304 stainless steel with H/Me = 1.03 (circles) and model calculation by Born–von Karman model, regarding the alloy as 'MeH monohydride' (crosses) and taking into account the broadening because of alloying effects (line).

Table 3. (Continued.)

Table 3.6: Force constants (in N m^{-1}) describing metal–hydrogen and hydrogen–hydrogen interactions for 310 stainless steel (Fe/Cr25/Ni20), considering the variation of vibrational energies because of the different metal atoms surrounding hydrogen atoms.

Notation	Interaction	Value (N m^{-1})	Parameter status
α_2	ϕ_{xx} (1/2, 0, 0) Me–H	32.6–61.8[b]	Fixed
α_3	ϕ_{xx} (1/2, 1/2, 0) H–H	7.6	Refined
β_3	ϕ_{zz} (1/2, 1/2, 0) H–H	1.6	Refined
γ_3	ϕ_{xz} (1/2, 1/2, 0) H–H	8.3	Refined

[a] Corresponding to maximum and minimum values for the various configurations of metal atoms in Fe/Cr18/Ni10 around hydrogen with probability over 1%.
[b] Corresponding to maximum and minimum values for the various configurations of metal atoms in Fe/Cr25/Ni20 around hydrogen with probability over 1%.

alloying compositions. The hydrogen vibrational energies for configurations with probability over 1% have been estimated by superposition from the results of ε'-FeH_1 (Cornell *et al* 1997), γ-$NiH_{1.05}$ (Kolesnikov *et al* 1991, Dorner *et al* 1989), ε-CrH_1 (Dorner *et al* 1989) for both steels. From the vibrational energies the metal–hydrogen force constants have been derived. For each configuration the phonon densities-of-states have been calculated, taking into account the instrumental resolution. The resulting phonon densities-of-states for 310 and 304 stainless steel have been derived by superposition of the corresponding values for the individual configurations. Figures 4 and 5 show the calculated and experimental densities-of-states for 304 steel with H/Me = 1.03 and 310 steel with H/Me = 0.94, respectively.

The model calculations show that the peak splitting into two components can be described by strong hydrogen–hydrogen interactions. Ignoring the force constants corresponding to hydrogen–hydrogen interactions resulted in asymmetric single peaks. Considering the influences of various alloying elements by superposition of different metal–hydrogen interactions leads to an improvement in the description of the experimental data. The small

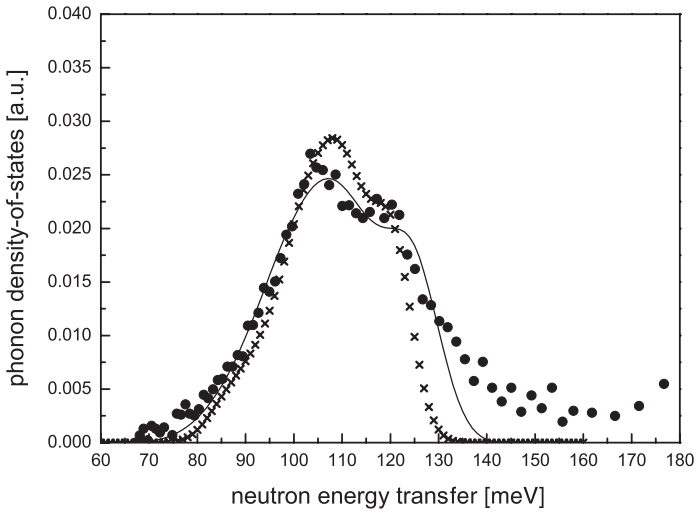

Figure 5. Phonon density-of-states of 310 stainless steel with H/Me = 0.94 (circles) and model calculation by Born–von Karman model, regarding the alloy as 'MeH monohydride' (crosses) and taking into account the broadening because of alloying effects (line).

discrepancies on the lower energy sides of the optical vibrational bands could result from scattering from ice. As the background resulting from fast neutrons increases strongly with increasing energy, the discrepancies between experimental and calculated data on the high-energy sides might be related to the quality of the background subtraction.

4. Conclusions

(1) In agreement with neutron diffraction data, the inelastic neutron scattering studies indicate that hydrogen atoms exclusively occupy the octahedral interstitial sites in 310 and 304 stainless steels for all hydrogen contents up to H/Me = 1.
(2) The spectra do not give any indications for a miscibility gap in the austenite hydride system for both steels. Indeed, no evidence for the coexistence of a hydride phase with the austenite matrix has been found.
(3) The obtained values for vibrational energies versus metal–hydrogen distance for H/Me $\approx$ 1 fit well with corresponding results found for pure metal hydrides of Ni, Fe, Cr and Mn.
(4) Increasing hydrogen contents, i.e. increasing metal–hydrogen distances, are accompanied by a softening of metal–hydrogen interactions.
(5) The peaks are broadened because of the variation of vibrational energies from one site to another in the alloys.
(6) At very high hydrogen concentrations, the broadening is dominated by hydrogen–hydrogen interactions, and a splitting of the peaks into transverse and longitudinal modes is observed.

Acknowledgments

Financial support from the Bundesministerium für Bildung und Forschung (German Ministry for Education and Science) is gratefully acknowledged. We thank V E Antonov and his co-workers from the Institute of Solid State Physics of the Russian Academy of Science in

Chernogolovka for their help in the high-pressure hydrogenations, as well as A I Kolesnikov (Argonne National Laboratory) for help in the inelastic neutron scattering studies.

References

Antonov V E, Cornell K, Dorner B, Fedotov V K, Grosse G, Kolesnikov A I, Wagner F E and Wipf H 2000 *Solid State Commun.* **113** 569–72

Cornell K, Wipf H, Antonov V E, Antonova T E, Kolesnikov A I, Ponyatovsky E G and Dorner B 1997 *Pol. J. Chem.* **71** 1792–6

Danilkin S A, Fuess H, Wipf H, Ivanov A, Gavriljuk V G, Delafosse D and Magnin T 2003 *Europhys. Lett.* **63** 69–75

Dawidowski J, Bermejo F J and Granada J R 1998 *Phys. Rev.* B **58** 706–15

Dorner B, Belash I T, Bokhenov E L, Ponyatovsky E G, Antonov V E and Pronina L N 1989 *Solid State Commun.* **69** 121–4

Elsässer C, Krimmel H, Fähnle M, Louie S G and Chan C T 1998 *J. Phys.: Condens. Matter* **10** 5131–46

Hoelzel M, Danilkin S A, Ehrenberg H, Toebbens D M, Udovic T J, Fuess H and Wipf H 2004 *Mater. Sci. Eng.* A **384** 255–61

Kolesnikov A I, Natkaniec I, Antonov V E, Belash I T, Fedotov V K, Krawczyk J, Mayer J and Ponyatovsky E G 1991 *Physica* B **174** 257–61

Li J and Kolesnikov A I 2002 *J. Mol. Liq.* **100/1** 1–39

Narita N, Altstetter C J and Birnbaum H K 1982 *Met. Trans.* **13A** 1355–65

Rajevac V, Hoelzel M, Danilkin S A, Hoser A and Fuess H 2004 *J. Phys.: Condens. Matter* **16** 2609–16

Ross D K 1997 Neutron scattering studies of metal hydrogen systems *Hydrogen in Metals III* (*Springer Topics in Applied Physics* vol 73) ed H Wipf (Berlin: Springer) pp 153–214

Ross D K, Martin P F, Oates W A and Khoda Bakhsh R 1979 *Z. Phys. Chem. NF* **114** 341–9

Udovic T J, Neumann D A, Leao J and Brown C M 2004 *Nucl. Instrum. Methods* A **517** 189–201

Ulmer D G and Altstetter C J 1993 *Acta Metall. Mater.* **41** 2235–41